SIMILARITY OF STRUCTURE-FUNCTION PARAMETERS IN THE STABLY STRATIFIED BOUNDARY LAYER

J. WYNGAARD and B. KOSOVIC
Department of Meteorology, Penn State University, University Park PA 16802-5013, USA

(Received in final form 12 April, 1994)

Abstract. The structure-function parameters C_T^2 and C_v^2 of temperature and velocity, respectively, from the 1973 Minnesota experiments and from large-eddy and direct numerical simulations show a smooth transition from M–O similarity to the "local scaling" hypothesized by Nieuwstadt for the outer regions of the stable boundary layer. Under that hypothesis, turbulence statistics aloft depend on the local vertical fluxes of momentum and temperature, so these results suggest that remote-sensing measurements of C_T^2 and C_v^2 could be used to infer vertical profiles of those fluxes. We argue that the sensitivity of the fluxes to unsteadiness, baroclinity, terrain slope, and breaking gravity waves precludes the universality of the vertical profiles of structure-function parameters in the stable PBL. We find that the C_T^2 profile is particularly sensitive to these effects, which is consistent with observations that it varies considerably from case to case.

1. Introduction

Many boundary-layer researchers will recall the impact of the McAllister *et al.* (1969) paper. These authors had pulsed an array of loudspeakers and detected the backscattered energy with the same array. By cleverly recording the signal on a facsimile receiver, they produced striking time-height displays showing how convective eddies rising from the heated surface in the early morning break up the nocturnal boundary layer. Use of the acoustic echo sounder, as it was soon called, spread rapidly.

Deardorff (1972) suggested that the acoustic echo sounder would be able to provide direct data on the nocturnal boundary-layer height h, a subject of speculation and controversy at that time. Similarity theories (e.g., Clarke, 1970) held that h satisfied the equilibrium relation

$$h = \left(\frac{cu_*}{f}\right) F\left(\frac{u_*}{fL}\right), \tag{1}$$

where $c \sim 0.3$, u_* is the friction velocity (the square root of the kinematic surface stress), f is the Coriolis parameter, and L is the Monin–Obukhov length; the function F is unity at neutral and decreases under stable stratification. It was not clear, however, whether the nocturnal boundary layer could reach this equilibrium. The behavior of conventional soundings of temperature and wind had led Blackadar (1957) to conclude that h typically increases during the night from its early-evening minimum.

On the basis of his one-dimensional model calculations, Deardorff inferred that h is generally time dependent and cannot be diagnosed from a steady-state

Boundary-Layer Meteorology **71:** 277–296, 1994.

similarity relation such as Equation (1). [He had just carried out time-dependent, fine-mesh, three-dimensional calculations of the neutral and convective PBLs; his attempts to extend these to the stable case failed because most of the turbulence became subgrid-scale. This approach, which we now call large-eddy simulation, or LES, was first applied successfully to the stable case by Mason and Derbyshire (1990).]

Rather than prescribing eddy-diffusivity profiles, as Deardorff had done in his model study, Delage (1974) used eddy diffusivities based on predicted turbulent kinetic energy. His one-dimensional model of the nocturnal boundary layer reached a steady state after several hours with a realistic rate of surface cooling. Wyngaard (1975), integrating a fuller set of second-moment equations, had similar findings. Brost and Wyngaard (1978), using a simplified form of Wyngaard's second-moment model, found that the stable boundary layer could reach an essentially steady state within a few hours.

Nieuwstadt (1984) showed that the Brost-Wyngaard equations have steady solutions displaying a similarity structure in outer regions that is an extension of Monin–Obukhov (M–O) similarity. In M–O similarity the friction velocity u_* and the surface temperature flux $\overline{\theta w_s}$ define the Obukhov length L:

$$L = -\frac{u_*^3}{k(g/T)\overline{\theta w_s}}. \tag{2}$$

Here k is the von Karman constant and g/T is the buoyancy parameter. The counterpart of L in "local scaling", as Nieuwstadt termed it, is the "local Obukhov length" Λ

$$\Lambda = -\frac{\tau^{3/2}}{k(g/T)\overline{\theta w}}, \tag{3}$$

where $\tau(z)$ is the magnitude of the local kinematic stress (i.e., $\tau^2(z) = \overline{uw}^2(z) + \overline{uw}^2(z)$) and $\overline{\theta w}(z)$ is the local temperature flux. Under Nieuwstadt's local-scaling hypothesis, quantities made dimensionless with τ, $\overline{\theta w}$, and Λ depend only on z/Λ. Nieuwstadt showed that observations taken in the nocturnal PBL at Cabauw, The Netherlands, support this hypothesis.

Nieuwstadt pointed out that local scaling is not very well suited for practical applications because it does not directly give vertical profiles of turbulence. However, one can obtain profiles by using local scaling as a closure in model equations for the stable boundary layer. With such a closure, one finds that the turbulence profiles depend on the time history of the boundary layer. As Wyngaard (1988) states, "... a simple, diagnostic similarity framework for the *structure* of the nocturnal boundary layer seems not to exist. What we have described instead is a relatively simple model of its *dynamics*.... (Its) solution ... gives the structure, which then depends on the history of the flow and boundary conditions."

2. The Structure-Function Parameters

2.1. Refractive index

Most theoretical analyses of the scattering of electromagnetic, acoustic, and optical radiation by turbulence use the refractive index structure function (Tatarskii, 1971) which is defined by

$$\overline{[n(\mathbf{x},t) - n(\mathbf{x}+\mathbf{r},t)]^2} \equiv \overline{(n-n')^2}, \tag{4}$$

where n is the fluctuating refractive index at point $\mathbf{x}$ and n' that at point $\mathbf{x}+\mathbf{r}$. The overbar denotes the ensemble average. Many problems of practical importance involve this structure function only for separations $r = \mid \mathbf{r} \mid$ in the inertial range of scales, where it has the form

$$\overline{(n-n')^2} = C_N^2 r^{2/3}. \tag{5}$$

Fluctuations in the refractive index for electromagnetic radiation are caused primarily by fluctuations in temperature and absolute humidity, θ and q, respectively. For fluctuation levels typical of the atmospheric boundary layer one can write

$$n = a\theta + bq, \tag{6}$$

where the coefficients a and b depend on the wavelength of the radiation. Wyngaard *et al.* (1978) have shown that this implies that C_N^2 may be expressed in terms of the structure-function parameters for temperature and humidity, C_T^2 and C_Q^2, and the joint parameter, C_{TQ}:

$$C_N^2 = a^2 C_T^2 + 2abC_{TQ} + b^2 C_Q^2. \tag{7}$$

(For acoustic radiation, C_N^2 depends also on the turbulent velocity field.) Functional forms for the coefficients in Equation (7) are summarized by Burk (1979) for acoustic, microwave, and optical radiation. Gossard (1988) has discussed the maintenance of the joint parameter C_{TQ} and its role in radar scattering.

These structure-function parameters are directly proportional to the spectra of temperature and humidity, and their cospectrum, respectively, in the inertial subrange. Similarity arguments due to Kolmogorov, Obukhov, and Corrsin (see Tennekes and Lumley, 1972) indicate that these inertial-range spectral levels depend only on the molecular destruction rates ϵ, χ_θ, χ_q, and $\chi_{\theta q}$ of turbulent kinetic energy, potential temperature and humidity variances, and their covariance, respectively. In the inertial range the one-dimensional spectra behave as (Wyngaard and LeMone, 1980):

$$\begin{aligned}
\Phi_T(\kappa_1) &= 2(2\pi)^{-1}\Gamma(5/3)\sin(\pi/3)C_T^2\kappa_1^{-5/3}, \\
&= 0.25C_T^2\kappa_1^{-5/3} = \beta_1\epsilon^{-1}\chi_\theta\kappa_1^{-5/3}, \\
Co_{TQ}(\kappa_1) &= 0.25C_{TQ}\kappa_1^{-5/3} = \gamma_1\epsilon^{-1/3}\chi_{\theta_q}\kappa_1^{-5/3}, \\
\Phi_Q(\kappa_1) &= 0.25C_Q^2\kappa_1^{-5/3} = \beta_1\epsilon^{-1/3}\chi_q\kappa_1^{-5/3},
\end{aligned} \tag{8}$$

where β_1 and γ_1 are the one-dimensional spectral constants. Our normalization in Equation (8) is such that the integral over the half-line is the covariance. Following Wyngaard and Lemone (1980), we take $\beta_1 = \gamma_1 = 0.4$ and recast Equation (8) as

$$\begin{aligned}
C_T^2 &= 1.6\epsilon^{-1/3}\chi_\theta, \\
C_{TQ} &= 1.6\epsilon^{-1/3}\chi_{\theta q}, \\
C_Q^2 &= 1.6\epsilon^{-1/3}\xi_q.
\end{aligned} \tag{9}$$

2.2. Velocity

As discussed by Kaimal (1973), the inertial-subrange form of the velocity structure function for u_1, for example, is

$$\overline{[u_1(\mathbf{x},t) - u_1(\mathbf{x}+\mathbf{r},t)]^2} = C_v^2 r^{2/3}, \tag{10}$$

where C_v^2 is called the velocity structure-function parameter. Kaimal presents the spectral relations analogous to Equation (8). We need only the result

$$C_v^2 = 4\alpha_1\epsilon^{2/3} \simeq 2\epsilon^{2/3}, \tag{11}$$

where $\alpha_1 \simeq 0.5$ is the one-dimensional spectral constant for velocity. When acoustic radiation is scattered at angles other than 180°, C_v^2 can be the dominant factor in the scattering cross-section.

3. Similarity Structure

Equations (9) and (11) tie the structure-function parameters to the rates of molecular destruction of the temperature-humidity covariances and of turbulent kinetic energy. We can relate these destruction rates to the dynamics of the turbulence through the second-moment equations. We derive these formally by using the ensemble mean, fluctuating decomposition for all random fields (Tennekes and Lumley, 1972). We denote these fields with a tilde, using upper and lower case symbols for their mean and fluctuating parts, respectively:

$$\tilde{u}_i = U_i + u_i; \quad \tilde{p} = P + p; \quad \tilde{T} = \Theta + \theta; \quad \tilde{q} = Q + q. \tag{12}$$

We shall use the mixed notation $u_i = (u_1, u_2, u_3) = (u, v, w)$; $x_i = (x_1, x_2, x_3) = (x, y, z)$.

Let us assume that conditions are locally homogeneous in the horizontal and quasi-steady, so that the mean advection and time-change terms in the second-moment equations are negligible. Satisfying these assumptions requires that the time and length scales of the turbulence are small compared to those of the external changes, which is often the case under clear conditions at good sites (Wyngaard, 1992). Then the budget of potential temperature variance is (Wyngaard and Coté, 1971):

$$2\overline{\theta w}\frac{\partial \Theta}{\partial z} + \frac{\partial \overline{\theta^2 w}}{\partial z} = -\chi_\theta, \tag{13}$$

The budgets of humidity variance and the temperature-humidity covariance are (Wyngaard *et al.*, 1978)

$$2\rho\overline{wq}\frac{\partial}{\partial z}\left(\frac{Q}{\rho}\right) + \frac{\partial \overline{q^2 w}}{\partial z} = -\chi_q, \tag{14}$$

$$\overline{wq}\frac{\partial \Theta}{\partial z} + \rho\overline{\theta w}\frac{\partial}{\partial z}\left(\frac{Q}{\rho}\right) + \frac{\partial \overline{\theta q w}}{\partial z} = -\chi_{\theta q}, \tag{15}$$

where ρ is the mean density. Finally, the turbulence kinetic energy (TKE) equation is

$$\overline{uw}\frac{\partial U}{\partial z} + \overline{vw}\frac{\partial V}{\partial z} + \frac{\partial}{\partial z}\frac{\overline{w u_i u_i}}{2} = \frac{1}{\rho}\frac{\partial \overline{pw}}{\partial z} + \frac{g}{T}\overline{\theta w} - \epsilon, \tag{16}$$

where repeated indices are summed. We are assuming here that the humidity is sufficiently small that it does not contribute significantly to buoyancy; if this is not the case, one can use the same equations but interpret $\tilde{T}$ as the virtual potential temperature (Lumley and Panofsky, 1964).

It seems generally agreed (Panofsky and Dutton, 1984) that to a good approximation in the quasi-steady, locally homogeneous surface layer, the budgets of scalar variance and turbulent kinetic energy reduce to a local balance between production and molecular destruction. The $\overline{\theta q}$ budget has not received as much attention, but Wyngaard *et al.* (1978) found that in the unstable surface layer, it also has a local balance. Since our experience with these second-moment budgets generally indicates that the turbulent transport (i.e., the third-moment divergence) terms are least important under stable conditions, it is plausible that the local balance for the $\overline{\theta q}$ budget extends to stable conditions as well. Thus, we write Equations (13)–(15) as

$$\chi_\theta = -2\overline{\theta w}\frac{\partial \Theta}{\partial z},$$

$$\chi_q = -2\rho\overline{qw}\frac{\partial}{\partial z}\left(\frac{Q}{\rho}\right),$$

$$\chi_{\theta q} = -\rho\overline{\theta w}\frac{\partial}{\partial z}\left(\frac{Q}{\rho}\right) - \overline{qw}\frac{\partial\Theta}{\partial z}. \tag{17}$$

The TKE Equation (16) becomes

$$\epsilon = -\overline{uw}\frac{\partial U}{\partial z} - \overline{vw}\frac{\partial V}{\partial z} + \frac{g}{T_0}\overline{\theta w}. \tag{18}$$

3.1. Surface-layer similarity

We use the conventional surface-layer temperature and humidity scales T_* and q_*,

$$T_* = -\frac{\overline{\theta w_s}}{u_*}, \quad q_* = -\frac{\overline{qw_s}}{u_*}, \tag{19}$$

where $\overline{qw_s}$ is the surface humidity flux. Under the M–O hypothesis for the quasi-steady, locally homogeneous surface layer, mean gradients made dimensionless with these scales and height z are universal functions of z/L:

$$\frac{kz}{T_*}\frac{\partial\Theta}{\partial z} = \phi_h(z/L),$$

$$\frac{kz}{q_*}\rho\frac{\partial}{\partial z}\left(\frac{Q}{\rho}\right) = \phi_q(z/L). \tag{20}$$

It is not clear whether the functions ϕ_h and ϕ_q differ; following Panofsky and Dutton (1984), we assume that they are equal. In the surface layer the fluxes of temperature, humidity, and momentum are essentially equal to their surface values, so under the M–O hypothesis we can write Equation (17) as

$$\chi_\theta = \frac{2}{k}\frac{u_*T_*^2}{z}\phi_h; \quad \chi_q = \frac{2}{k}\frac{u_*q_*^2}{z}\phi_h; \quad \chi_{\theta q} = \frac{2}{k}\frac{u_*T_*q_*}{z}\phi_h. \tag{21}$$

We choose the x-axis along the mean wind, so that $U_i = [U(z), 0, 0]$ and the M–O function for mean wind shear is

$$\phi_m(z/L) = \frac{kz}{u_*}\frac{\partial U}{\partial z}. \tag{22}$$

We can write the dissipation-rate expression (18) as

$$\epsilon = \frac{u_*^3}{kz}(\phi_m - z/L). \tag{23}$$

Combining Equations (9), (21), and (23) then yields M–O expressions for the refractive index structure-function parameters:

$$\frac{C_T^2 z^{2/3}}{T_*^2} = \frac{C_Q^2 z^{2/3}}{q_*^2} = \frac{C_{TQ} z^{2/3}}{q_* T_*} = \frac{3.2}{k^{2/3}} \phi_h (\phi_m - z/L)^{-1/3}. \tag{24}$$

That for velocity is

$$\frac{C_v^2 z^{2/3}}{u_*^2} = \frac{2}{k^{2/3}} (\phi_m - z/L)^{2/3}. \tag{25}$$

Unlike the other structure parameters, C_{TQ} is not positive definite; its sign is that of $T_* q_*$ – i.e., that of the product of the surface fluxes of temperature and humidity. Under stably stratified conditions, the surface temperature flux is negative; we would normally expect the surface humidity flux to be positive, so C_{TQ} is negative under typical stable conditions.

Of the three refractive-index structure-function parameters, only C_T^2 has been measured extensively. The Kansas results (Businger *et al.*, 1971) indicate for stable conditions

$$\phi_h = 0.74 + 4.7 z/L; \quad \phi_m = 1.0 + 4.7 z/L, \tag{26}$$

so that with the Kansas value of 0.35 for k, the M–O form Equation (24) for C_T^2 becomes

$$\frac{C_T^2 z^{2/3}}{T_*^2} = \frac{4.8(1 + 6.35 z/L)}{(1 + 3.7 z/L)^{1/3}}. \tag{27}$$

Figure 1 shows C_T^2 data from the 1968 Kansas experiments (Wyngaard *et al.*, 1971), the 1973 Minnesota experiments (Caughey *et al.*, 1979), and experiments reported by Foken and Kretschmer (1990). Equation (27) fits those results fairly well.

3.2. The stable surface-layer asymptote

Under very stable conditions (large z/L), expression (27) for C_T^2 becomes

$$\frac{C_T^2 z^{2/3}}{T_*^2} \simeq 20 (z/L)^{2/3}. \tag{28}$$

Equation (25) for C_v^2 becomes, using Equation (26),

$$\frac{C_v^2 z^{2/3}}{u_*^2} \simeq 9.6 (z/L)^{2/3}. \tag{29}$$

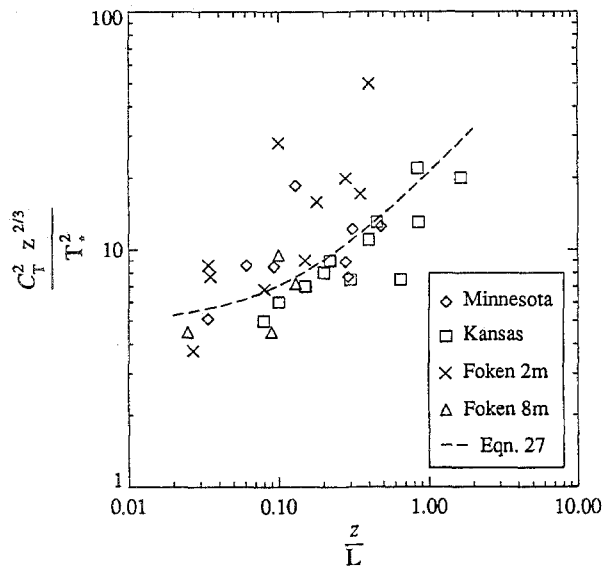

Fig. 1. Experimental data on C_T^2 in the stable surface layer, presented in M–O coordinates.

In this limit, the structure-function parameters are independent of z:

$$C_T^2 \simeq 20\frac{T_*^2}{L^{2/3}}, \quad C_v^2 \simeq 9.6\frac{u_*^2}{L^{2/3}}. \tag{30}$$

A "local z-less stratification" interpretation of Equation (30) (Wyngaard, 1973) is that under very stable conditions, turbulent eddy sizes are restricted by stability and z loses significance as a length scale for the turbulence. Then the only length scale is L, the only temperature scale is T_*, and the only velocity scale is u_*, so that C_T^2 and C_v^2 must scale with $T_*^2/L^{2/3}$ and $u_*^2/L^{2/3}$, respectively.

3.3. Outer-layer similarity

Let us briefly review the physics underlying the notion of local scaling of turbulence in the stably stratified boundary layer and the evidence supporting it.

When the requisite turbulence sensors and data-acquisition systems became available by the 1960s, researchers studied in detail the structure of the surface layer and the transport processes within it over a wide range of stability conditions. Under stable conditions, the second-moment budgets showed a local equilibrium state in which the turbulent transport (third-moment flux divergence) terms were small and the production and destruction rates were in balance, as exhibited in Equations (17) and (18). Furthermore, the data behaved as if L rather than z determined the length scale of the turbulence under very stable conditions, as exhibited in Equation (30). These findings stood in striking contast with those for the unstable surface layer.

Numerical models that used closures rooted in this interpretation of stable surface-layer physics appeared (Delage, 1974; Brost and Wyngaard, 1978; Nieuwstadt, 1984). There were indications that such models could account fairly well for observed behavior (Caughey *et al.*, 1979; Nieuwstadt, 1984), although flow intermittency under very stable conditions (Kondo *et al.*, 1978) and gravity-wave effects (de Baas and Driedonks, 1985) were not generally accounted for by the models.

When the stably stratified boundary layer yielded to large-eddy simulation (Mason and Derbyshire, 1990), a new avenue to studying its structure and dynamics was opened. Derbyshire (1990) suggested that a key parameter is $B_0/(G^2 f)$, where B_0 is the surface buoyancy flux and G is the magnitude of the geostrophic wind. He argued that when $B_0/(G^2 f) \leq 0.1$, approximately, the layer can exist in a quasi-steady state. Regarding gravity waves, Mason and Derbyshire stated that "The potentially nonlocal character of some wave motions does not seem to be strong enough to invalidate local scaling. ... Arguments given by Derbyshire (1990) show that this is to be expected if the waves are generated purely by turbulence, though topographic waves may of course behave differently." In the quasi-steady state and without topography, the Mason-Derbyshire results indicate broad agreement with the local-scaling hypothesis for the nocturnal boundary layer.

Under the local scaling hypothesis we can write for the outer layer

$$\widetilde{C_T^2} = \frac{C_T^2 \tau \Lambda^{2/3}}{\overline{\theta w}^2} = f_1(z/\Lambda), \quad \widetilde{C_v^2} = \frac{C_v^2 \Lambda^{2/3}}{\tau} = f_2(z/\Lambda), \tag{31}$$

where f_1 and f_2 are functions to be determined. The vanishing significance of z under strong stratification implies that f_1 and f_2 approach constants in the limit $z/\Lambda \to \infty$, as do the flux and gradient Richardson numbers. The Brost-Wyngaard model gives in this stable limit

$$\widetilde{C_T^2} = f_1 = \frac{6.2\widetilde{\overline{w^2}}^{1/6}}{\tilde{K}_h^{5/6} \tilde{E}^{1/2}}, \quad \widetilde{C_v^2} = f_2 = \frac{0.54\tilde{E}}{\widetilde{\overline{w^2}}^{1/3} \tilde{K}_h^{1/3}}, \tag{32}$$

where K_h is the eddy diffusivity for temperature, E is twice the turbulent kinetic energy per unit mass, and a tilde denotes nondimensionalization with the local scales $\overline{\theta w}$, τ, and Λ. Each of these dimensionless dependent variables is a function of z/Λ. Nieuwstadt's numerical solutions show that as z/Λ increases, they approach constant values of

$$\tilde{K}_h \simeq 0.08, \quad \tilde{E}^{1/2} \simeq 2.9, \quad \widetilde{\overline{w^2}} \simeq 1.7, \tag{33}$$

so that from Equation (32)

$$f_1 \simeq 19, \quad f_2 \simeq 9, \tag{34}$$

and

$$C_T^2 \simeq 19\frac{(\overline{w\theta})^2}{\tau \Lambda^{2/3}}, \quad C_v^2 \simeq 9\frac{\tau}{\Lambda^{2/3}}. \tag{35}$$

These agree well with the surface-layer asymptotes in Equation (30) because the closure constants in the Brost-Wyngaard model were chosen so that its results were compatible with this stable limit. This is consistent with Sorbjan's (1986) hypothesis that for a given variable the forms of the M–O and outer-layer similarity functions are the same.

We tested the predictions (35) of the local-scaling hypothesis with results from both large-eddy and direct numerical simulation and with experimental data. The LES data, from the Mason-Derbyshire (1990) study of the stably stratified boundary layer, were provided to us by S. Derbyshire directly in the form of the molecular destruction rates and other statistical parameters. They used a domain 500 m in the direction of the geostrophic wind, 300 m wide, and 1000 m deep. Their numerical grid was $40 \times 32 \times 62$ points. The direct numerical simulation (DNS) data are from case SA of Coleman *et al.* (1992), who simulated a boundary layer over a cooled surface with a numerical grid having $96 \times 96 \times 45$ points. The flow was very low Reynolds number; GD/ν, where the laminar Ekman-layer depth, $D = \sqrt{2\nu/f}$, was 400. For air at midlatitudes, this corresponds to $G \sim 1$ cm s^{-1}. By contrast, this Reynolds number for an atmospheric case is about 400,000, 3 orders of magnitude larger. We accessed the DNS data base from G. Coleman and computed the statistics, averaging over horizontal planes and over five different times. We performed the calculations on the Cray-YMP at NCAR.

The LES data indicate that $\widetilde{C_T^2}$ approaches an asymptote of about 12 (Figure 2), while the DNS data suggest an asymptote perhaps 50% larger. For $\widetilde{C_v^2}$, the LES data show an asymptote of about 7 (Figure 3), while the DNS asymptote is again about 50% larger. This difference between the LES and DNS results could be due to the small Reynolds number of the DNS. Nonetheless, these asymptotes agree fairly well with those of Equation (35).

The experimental data were taken at $0.3 < z/h < 0.75$ in the 1973 Minnesota experiment (Caughey *et al.*, 1979). Unfortunately, only $\overline{uw}$ data are available; the lateral stress $\overline{vw}$ was contaminated by balloon motion. Thus, in calculating the local scaling parameter τ we neglected the contribution of $\overline{vw}$, which is difficult to justify near h. The Minnesota C_T^2 and C_v^2 data so scaled are plotted in Figures 4 and 5, respectively. In general they agree well with the local-scaling results Equation (35) and the results from the numerical simulations.

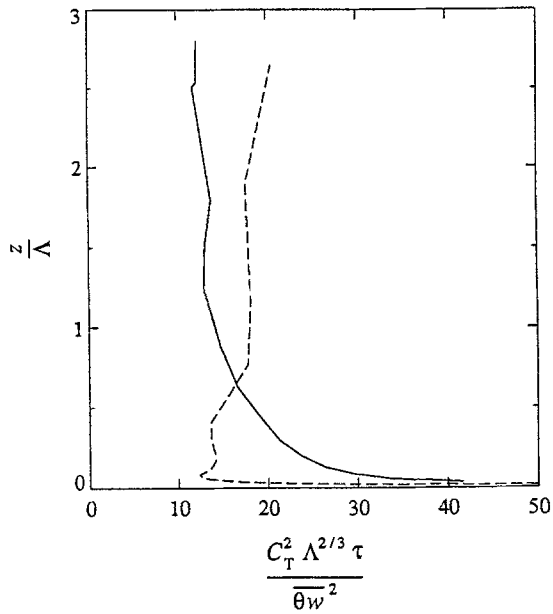

Fig. 2. C_T^2 data from numerical simulations of the nocturnal boundary layer, presented in local-scaling coordinates. —, Mason-Derbyshire LES; - - - - -, Coleman *et al.* DNS.

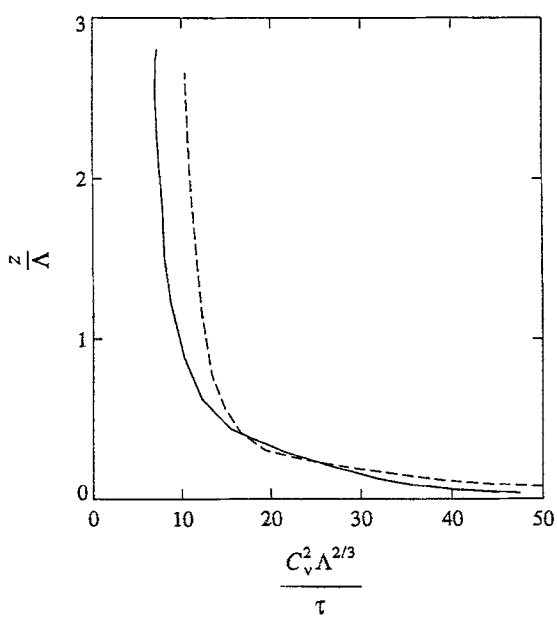

Fig. 3. C_v^2 data from numerical simulations of the nocturnal boundary layer, presented in local-scaling coordinates. —, Mason-Derbyshire LES; - - - - -, Coleman *et al.* DNS.

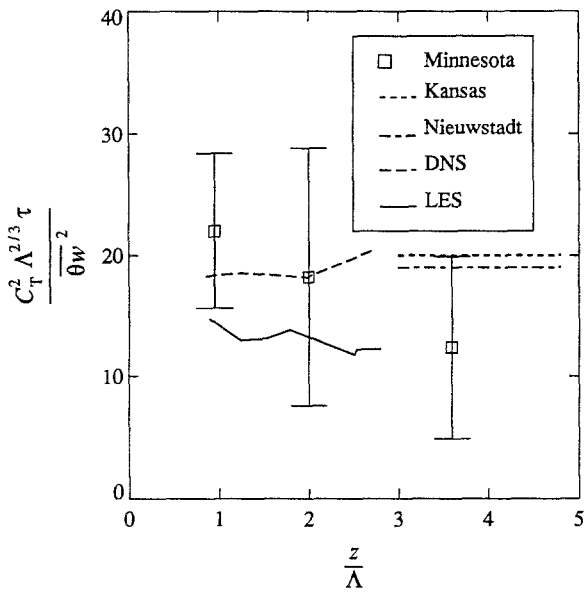

Fig. 4. A test of the local-scaling prediction that the dimensionless C_T^2 approaches a constant. The Minnesota data are averages over a few measurements; the symbol represents the mean and the bracket indicates plus and minus one standard error.

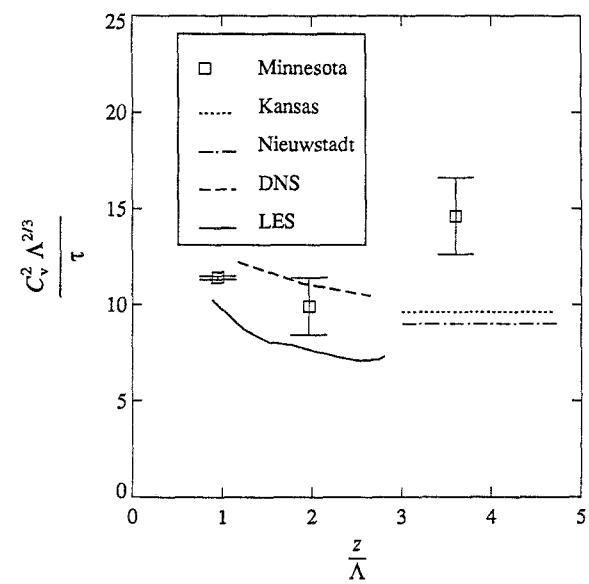

Fig. 5. A test of the local-scaling prediction that the dimensionless C_v^2 approaches a constant.

4. Vertical Profiles

From Equations (30) and (35) we have similarity relations for the vertical profiles of C_T^2 and C_v^2 over most of the stable boundary layer. From the outer edge of the surface layer through the outer layer we can write

$$C_T^2(z) \simeq 20 \left(k \frac{g}{T}\right)^{2/3} \frac{|\overline{\theta w}|^{8/3}}{\tau^2}, \quad C_v^2(z) \simeq 9 \left(\frac{kg}{T}\right)^{2/3} |\overline{\theta w}|^{2/3} . \tag{36}$$

The key ingredients in these similarity relations are the vertical profiles of kinematic stress magnitude $\tau(z)$ and temperature flux $\overline{\theta w}(z)$. The C_T^2 profile depends on both $\tau(z)$ and $\overline{\theta w}(z)$; their effects are opposite, and we shall argue later that their balance is so delicate that C_T^2 can either increase or decrease with height. By contrast, the profile of C_v^2 depends only on the $\overline{\theta w}$ profile and we expect both to decrease monotonically with height. Let us now consider the behavior of the τ and $\overline{\theta w}$ profiles in more detail.

4.1. Ideal (quasi-steady, horizontally homogeneous) conditions

In the simplest quasi-steady case with horizontal homogeneity and z-independent geostrophic wind components U_g and V_g, the equations for the evolution of the vertical gradients of mean wind and temperature reduce to

$$\frac{\partial^2 \overline{uw}}{\partial z^2} = f\frac{\partial V}{\partial z}, \quad \frac{\partial^2 \overline{vw}}{\partial z^2} = -f\frac{\partial U}{\partial z}, \tag{37}$$

$$\frac{\partial^2}{\partial z^2}\overline{\theta w} = 0. \tag{38}$$

With the boundary conditions $\overline{\theta w} = \overline{\theta w}_s$ at $z = 0$ and $\overline{\theta w} = 0$ at $z = h$, Equation (38) yields the steady-state $\overline{\theta w}$ profile

$$\overline{\theta w} = \overline{\theta w}_s(1 - z/h). \tag{39}$$

Nieuwstadt (1984) showed also that a stress closure based on local scaling gives a solution of Equation (37) whose τ profile is

$$\tau = u_*^2(1 - z/h)^{3/2}. \tag{40}$$

It follows from Equation (36) that the corresponding profiles of C_T^2 and C_v^2 from the outer edge of the surface layer through the outer layer are

$$C_T^2 \simeq 20\frac{T_*^2}{L^{2/3}}(1 - z/h)^{-1/3}, \quad C_v^2 \simeq 9\frac{u_*^2}{L^{2/3}}(1 - z/h)^{2/3}. \tag{41}$$

Equation (41) predicts that C_T^2 increases with height, but the observations of Caughey *et al.* (1979) and Cuijpers and Koshiek (1989) show that it decreases. The prediction of Equation (41) of an increasing C_T^2 profile results from the balance between the competing effects of $\overline{\theta w}$, which causes C_T^2 to decrease with height, and τ, which causes it to increase. Let us now examine other factors that can influence the shapes of the $\overline{\theta w}$ and τ profiles and, hence, change this balance.

4.2. Departures from ideal conditions

Since the stress and temperature flux profiles enter the mean balances of horizontal momentum and potential temperature, respectively, their shapes can depend on the many influences on these balances that appear under less than ideal micrometeorological conditions. Let us consider a few of these influences. For simplicity we shall investigate them in isolation – i.e., one at a time.

4.2.1. Time Changes

During its early phases, the nocturnal PBL must be unsteady. Near sundown the changing surface energy balance causes the surface heat flux to change from positive to negative; in a horizontally homogeneous case, the mean potential temperature gradient in the air above must then evolve according to

$$\frac{\partial}{\partial t}\frac{\partial \Theta}{\partial z} + \frac{\partial^2 \overline{\theta w}}{\partial z^2} = 0. \tag{42}$$

In the initial stages of evolution, $\partial\Theta/\partial z$ grows in time, so that $\partial^2\overline{\theta w}/\partial z^2$ is negative. Let us now estimate the departures from a linear $\overline{\theta w}$ profile that this causes.

Let us model the $\overline{\theta w}$ profile in the evolving nocturnal PBL as

$$\overline{\theta w} = \overline{\theta w}_s \left(1 - \frac{z}{h}\right) + 4\delta\overline{\theta w}\frac{z}{h}\left(1 - \frac{z}{h}\right), \tag{43}$$

where $\delta\overline{\theta w}$ is the midlayer departure from a linear profile. We scale the terms in the mean temperature evolution equation as

$$\frac{\partial^2 \overline{\theta w}}{\partial z^2} = -\frac{8\delta\overline{\theta w}}{h^2}, \quad \frac{\partial}{\partial t}\frac{\partial \Theta}{\partial z} \sim \frac{1}{\tau_g}\frac{\partial \Theta}{\partial z}, \tag{44}$$

where τ_g is a time scale of the evolution of the mean potential temperature gradient. Thus, the balance Equation (42) is

$$\frac{\delta\overline{\theta w}}{\overline{\theta w}_s} \sim \frac{1}{\tau_g}\frac{\partial \Theta}{\partial z}\frac{h^2}{8\overline{\theta w}_s} \sim \frac{h\Delta\Theta}{8\tau_g\overline{\theta w}_s}, \tag{45}$$

where Δ denotes the change across the boundary layer. For typical values of h = 200 m, $\Delta\Theta$ = 5 K, τ_g = 12 h, and $\overline{\theta w}_s = -0.01$ m K s^{-1}, Equation (45) yields $\delta\overline{\theta w}/\overline{\theta w}_s \simeq -1/4$. Then to a good approximation, the $\overline{\theta w}$ profile (43) becomes in this case

$$\overline{\theta w} \simeq \overline{\theta w}_s \left(1 - \frac{z}{h}\right) - \overline{\theta w}_s \frac{z}{h}\left(1 - \frac{z}{h}\right) = \overline{\theta w}_s \left(1 - \frac{z}{h}\right)^2. \tag{46}$$

The data on $\overline{\theta w}$ from the rapidly evolving, early-evening boundary layers in the Minnesota experiment (Caughey *et al.*, 1979) are fit well by Equation (46).

It appears that this time-change-induced departure from linearity of the $\overline{\theta w}$ profile can have a strong effect on C_T^2. Consider, for example, a situation where τ behaves as $(1 - z/h)^{3/2}$, as in Equation (40). Then Equation (36) shows that a linear $\overline{\theta w}$ profile gives C_T^2 increasing as $(1 - z/h)^{-1/3}$, while a parabolic $\overline{\theta w}$ profile yields C_T^2 decreasing as $(1 - z/h)^{-7/3}$. Put another way, for a given

τ profile, Equation (36) shows that the ratio of C_T^2 for linear and parabolic $\overline{\theta w}$ profiles varies as $(1 - z/h)^{-8/3}$, which translates to an order-of-magnitude difference in C_T^2 values at $z/h \sim 0.6$.

Under unsteady but horizontally homogeneous conditions, the z-derivatives of mean horizontal momentum equations are

$$\frac{\partial^2 \overline{uw}}{\partial z^2} = f\frac{\partial V}{\partial z} - \frac{\partial}{\partial t}\frac{\partial U}{\partial z}, \quad \frac{\partial^2 \overline{vw}}{\partial z^2} = -f\frac{\partial U}{\partial z} - \frac{\partial}{\partial t}\frac{\partial V}{\partial z}. \tag{47}$$

We can define a time scale τ_s of the evolution of mean shear in analogy with τ_g, the time scale for evolution of the mean temperature gradient in Equation (44). We see from Equation (47) that if $f\tau_s \sim 1$, the evolving mean shear can have a significant effect on the stress profile curvature. Since the time scale for adjustment of the mean wind profiles to the decaying turbulent stress divergence in the late afternoon and early evening is $1/f$, it appears that $f\tau_s$ could be of order 1 at those times.

4.2.2. Baroclinity

Let the flow be steady and horizontally homogeneous except for mean temperature gradients in x and y. The vertical gradients of U_g and V_g are given hydrostatically by

$$\frac{\partial U_g}{\partial z} = -\frac{g}{fT}\frac{\partial T}{\partial y}, \quad \frac{\partial V_g}{\partial z} = \frac{g}{fT}\frac{\partial T}{\partial x}. \tag{48}$$

The mean-shear equations are now

$$\frac{\partial^2 \overline{uw}}{\partial z^2} = f\left(\frac{\partial V}{\partial z} - \frac{\partial V_g}{\partial z}\right), \quad \frac{\partial^2 \overline{vw}}{\partial z^2} = f\left(-\frac{\partial U}{\partial z} + \frac{\partial U_g}{\partial z}\right). \tag{49}$$

The terms on the right side represent the rate of generation of mean wind shear by Coriolis forces and baroclinity, respectively; in steady conditions, they balance the stress curvature.

The mean potential temperature gradient balance now becomes

$$\frac{\partial^2 \overline{w\theta}}{\partial z^2} = \frac{fT}{g}\left(\frac{\partial V}{\partial z}\frac{\partial U_g}{\partial z} - \frac{\partial U}{\partial z}\frac{\partial V_g}{\partial z}\right). \tag{50}$$

The right side represents the rate of generation of vertical gradients of potential temperature by the interaction of mean wind shear and the horizontal temperature gradient, which has been written in terms of the baroclinity through Equation (48).

Equation (49) shows that the stress profile curvature will be significantly modified by baroclinity if the geostrophic wind shear is an appreciable fraction of the wind shear. According to Equation (48), in midlatitudes a horizontal temperature

gradient of 3 K per 100 km, not an unusually large value, causes a geostrophic wind shear of 10 m s^{-1} per km. This is comparable to the wind shear, so we conclude that typical magnitudes of baroclinity can indeed have a substantial effect on the curvature of the stress profile.

Equation (50) shows that baroclinity also induces curvature of the $\overline{\theta w}$ profile. Let us estimate the geostrophic wind shear required to generate a significant departure from a linear profile. Denoting the magnitude of the mean wind as S, we use Equation (43) as a model of the $\overline{\theta w}$ profile and scale the terms in Equation (50) as:

$$\frac{8\delta\overline{w\theta}}{h^2} \sim \frac{fT}{g}\frac{\Delta S}{h}\frac{\Delta G}{h}. \tag{51}$$

It follows that the fractional change in midlayer temperature flux with respect to a linear profile is

$$\frac{\delta\overline{w\theta}}{\overline{\theta w}_s/2} = \frac{fT}{4g}\frac{\Delta S \Delta G}{\overline{\theta w}_s}. \tag{52}$$

For $\overline{\theta w}_s = -0.01$ m s^{-1} K and $\Delta S \Delta G = 10$ m^2 s^{-2}, Equation (52) gives a 70% change in the mid-layer temperature flux. We conclude that moderate baroclinity can appreciably change the $\overline{\theta w}$ profile.

4.2.3. Terrain Slope

Consider a nocturnal PBL that is homogeneous in planes parallel to a land surface that slopes at an angle β to the horizontal. Then the steady mean wind gradient equations in coordinates aligned with the sloping terrain are (Brost and Wyngaard, 1978)

$$\frac{\partial^2\overline{uw}}{\partial z^2} = f\frac{\partial V}{\partial z} - \frac{g}{T}\frac{\partial\Theta}{\partial z} \mid \beta \mid \cos\gamma,$$
$$\frac{\partial^2\overline{vw}}{\partial z^2} = -f\frac{\partial U}{\partial z} + \frac{g}{T}\frac{\partial\Theta}{\partial z} \mid \beta \mid \sin\gamma. \tag{53}$$

Here γ is the angle, measured counterclockwise, from the fall-line vector (the vector perpendicular to the contour lines and pointing down the slope) to the x-axis. Let us use Equation (53) to estimate the threshold terrain slope that gives a drainage term that appreciably changes the stress profile. We can do this simply by equating the magnitudes of the drainage and Coriolis terms. This yields

$$\beta \sim \frac{fT\Delta S}{g\Delta\Theta}. \tag{54}$$

For $\Delta S = 10$ m s^{-1} and $\Delta\Theta = 5$ K, this gives $\beta \sim 1.5 \times 10^{-3}$, a terrain slope of 1.5 parts per thousand. This is the slope of the unusually flat Minnesota site (Caughey *et al.*, 1979). We conclude that terrain-slope effects on the stress profile are apt to be significant.

4.2.4. Internal Gravity Waves

De Baas and Driedonks (1985) observed nocturnal PBL structure from the 200-m tower at Cabauw, The Netherlands. On occasion they detected Kelvin-Helmholtz waves with frequencies in the range 3×10^{-3} Hz to 2×10^{-3} Hz that persisted as quasi-steady oscillations for as long as one hour without breaking into turbulence. Their presence was seen not only in the time series of fluctuations, but also in the increase of the vertical velocity and temperature variance with height.

Einaudi and Finnigan (1981) analyzed a nearly monochromatic wave of 240 s period detected in a weakly stable, nocturnal boundary layer at the Boulder Atmospheric Observatory. They found that linear wave theory described the wave properties and the vertical structure of the w and θ fluctuations well. In a second paper (Finnigan and Einaudi, 1981) they showed that while the wave-like fluctuations in Reynolds stress were larger than the background turbulent stress levels, they were nearly in quadrature with the gradients of wave velocity, so they did not extract energy from the wave at an appreciable rate; as a result, the wave could persist in a quasi-steady state. They found that the turbulence time scale was longer than the wave period, however, so the turbulence was not in equilibrium with the large, wave-frequency fluctuations in shear production.

Coulter (1990) found that the turbulence levels in the nocturnal PBL over gently rolling terrain in northeastern Illinois were quite different on consecutive nights with similar mean conditions. Turbulence levels were low on the first night, but during the second night the signals showed evidence of waves of 2-min period that grew and extended beyond the PBL depth at approximately 60-min intervals. The records showed clearly defined active and inactive periods, with the differences in turbulence parameters σ_w, N, and ϵ ranging from a factor of 2 to 4 between them. Coulter interpreted the 2-min periodicities as Kelvin-Helmholtz waves made detectable to the acoustic sounder through their modulation of the local turbulence structure. He inferred that they grew rapidly in amplitude with time until they overturned and broke into turbulence that temporarily erased the wind shear and temperature gradient. Within about 30 minutes, the cycle was renewed.

These studies indicate that the nocturnal PBL can have strong gravity-wave activity that modifies its turbulence structure. In view of the Finnigan-Einaudi finding that the time scales of the wave and the turbulence can be of the same order, we must conclude that the local-scaling relations for structure-function parameters could be modified as well. For this reason, in his analysis Nieuwstadt (1984) excluded cases with strong gravity waves by including only those for which $\overline{w^2}$ decreased continuously with height. He then used a high-pass filter on the time series, as did Caughey *et al.* (1979).

4.3. Implications for Remote Sensing

We have argued that the sensitivity of structure-function parameter profiles in the stable PBL to flow unsteadiness, baroclinity, terrain slope, and internal gravity

waves precludes the universality of these profiles in the typical nocturnal case. This is consistent with the findings of Cuijpers and Koshiek (1988). Their measured C_T^2 profiles in the nocturnal boundary layer were not fit well by the steady state models of Nieuwstadt (1984, 1985) or Sorbjan (1986). The numerical model of Duynkerke and Driedonks (1987), which uses closures similar to those of Nieuwstadt but allows for time evolution of the boundary layer, gave the best results.

At the same time, the similarity expressions (36) that relate the structure-function parameters to local values of turbulent stress and temperature flux are consistent with observations, LES results, and model predictions. Thus, the evidence suggests that the similarity relations coupling the structure-function parameters to the turbulence are more robust than similarity relations for the vertical profiles of structure-function parameters. We interpret this as a characteristic of the turbulence dynamics underlying the second-moment Equations (13)–(16); evidently the spatial and temporal scales of that turbulence are sufficiently small that this dynamics is not substantially affected by slower and larger-scale changes in the background conditions.

This has interesting implications for remote sensing. From the second of Equation (36), we see that a measurement of C_v^2 yields the temperature flux directly:

$$\overline{\theta w} = -\frac{0.037T}{kg}(C_v^2)^{3/2}. \tag{55}$$

A measurement of C_T^2 as well then yields the stress magnitude from the first of Equation (36):

$$\tau = \frac{0.055T}{kg}\frac{(C_v^2)^2}{(C_T^2)^{1/2}}. \tag{56}$$

Neff and Coulter (1986) and Gossard (1992) have discussed the measurement of structure-parameter profiles with ground-based remote sensors.

If the measured C_T^2 and C_v^2 have errors $\epsilon(C_T^2)$ and $\epsilon(C_v^2)$, then from Equations (55) and (56) the errors in the inferred fluxes are, to first order,

$$\frac{\epsilon(\overline{w\theta})}{\overline{w\theta}} = \frac{3}{2}\frac{\epsilon(C_v^2)}{C_v^2}, \quad \frac{\epsilon(\tau)}{\tau} = 2\frac{\epsilon(C_v^2)}{C_v^2} - \frac{1}{2}\frac{\epsilon(C_T^2)}{C_T^2}, \tag{57}$$

showing that the technique is considerably more sensitive to errors in C_v^2 than in C_T^2.

5. Conclusion

The local-scaling hypothesis holds that over most of the nocturnal boundary layer, the turbulence is near its critical Ricardson number and its length, velocity,

and temperature scales are determined by the local stress and buoyancy flux. Data from several field experiments and both direct and large-eddy simulations show that the structure-function parameters for temperature and velocity are consistent with local scaling. The vertical profiles of the structure-function parameters are apt to be highly variable because of the sensitivity of the stress and temperature flux profiles to unsteadiness of the flow, baroclinity, terrain slope, and gravity waves. The local scaling result does offer the prospect that the stress and temperature flux profiles can be inferred from measurements of the structure-function parameter profiles, however.

Acknowledgments

The authors are grateful to Drs. P. J. Mason and S. H. Derbyshire for providing us with their LES data; to Dr. G. Coleman for providing his DNS data; to Drs. E. Andreas, D. Thomson, and J. Peltier for helpful discussions; and to the Geophysical Turbulence Program of the National Center for Atmospheric Research for providing computer time. This work was supported by the U.S. Army Research Office.

References

Blackadar, A. K.: 1957, 'Boundary-Layer Wind Maxima and Their Significance for the Growth of Nocturnal Inversions', *Bull. Amer. Meteorol. Soc.* **38**, 283–290.

Brost, R. A. and Wyngaard, J. C.: 1978, 'A Model Study of the Stably Stratified Planetary Boundary Layer', *J. Atmos. Sci.* **35**, 1427–1440.

Burk, S. D.: 1979, 'Refractive Index Structure Parameters: Time-Dependent Calculations Using a Numerical Boundary-Layer Model', *J. Appl. Meteorol.* **19**, 562–576.

Businger, J. A., Wyngaard, J. C., Izumi, Y., and Bradley, E. F.: 1971, 'Flux-Profile Relationships in the Atmospheric Surface Layer', *J. Atmos. Sci.* **28**, 181–189.

Caughey, S. J., Wyngaard, J. C., and Kaimal, J. C.: 1979, Turbulence in the Evolving Stable Boundary Layer', *J. Atmos. Sci.* **36**, 1041–1052.

Clarke, R. H.: 1970, 'Observational Studies in the Atmospheric Boundary Layer', *Quart. J. Roy. Meteorol. Soc.* **96**, 91–114.

Coleman, G. N., Ferziger, J. H., and Spalart, P. R.: 1992, 'Direct Simulation of the Stably Stratified Turbulent Ekman Layer', *J. Fluid Mech.* **244**, 667–690.

Coulter, R. L.: 1990, 'A Case Study of Turbulence in the Stable Nocturnal Boundary Layer', *Boundary-Layer Meteorol.* **52**, 75–91.

Cuijpers, J. W. M. and Koshiek, W.: 1989, 'Vertical Profiles of the Structure Parameter of Temperature in the Stable, Nocturnal Boundary Layer', *Boundary-Layer Meteorol.* **47**, 111–129.

Deardorff, J. W.: 1972, 'Rate of Growth of the Nocturnal Boundary Layer', in H. W. Church and R. E. Luna (eds.), *Proceeding of the Symposium on Air Pollution, Turbulence and Diffusion, December, 1971*, Sandia Laboratories, Albuquerque, NM.

de Baas, A. F. and Driedonks, A. G. M.: 1985, 'Internal Gravity Waves in a Stably Stratified Boundary Layer', *Boundary-Layer Meteorol.* **31**, 303–323.

Delage, Y.: 1974, 'A Numerical Study of the Nocturnal Atmospheric Boundary Layer', *Quart. J. Roy. Meteorol. Soc.* **100**, 351–364.

Derbyshire, S. H.: 1990, 'Nieuwstadt's Stable Boundary Layer Revisited', *Quart. J. Roy. Meteorol. Soc.* **116**, 127–158.

Einaudi, F. and Finnigan, J. J.: 1981, 'The Interaction between an Internal Gravity Wave and the Planetary Boundary Layer. Part I: The Linear Analysis', *Quart. J. Roy. Meteorol. Soc.* **107**, 793–806.

Finnigan, J. J. and Einaudi, F.: 1981, 'The Interaction between an Internal Gravity Wave and the Planetary Boundary Layer. Part II: Effect of the Wave on the Turbulence Structure', *Quart. J. Roy. Meteorol. Soc.* **107**, 807–832.

Foken, T. and Kretschmer, D.: 1990, 'Stability Dependence of the Temperature Structure Parameter', *Boundary-Layer Meteorol.* **53**, 185–189.

Gossard, E. E.: 1988, 'Measuring Gradients of Meteorological Properties in Elevated Layers with a Surface-Based Doppler Radar', *Radio Science* **23**, 625–639.

Gossard, E. E.: 1992, 'Relationship of Height Gradients of Passive Atmospheric Properties to their Variances: Applications to the Ground-Based Remote Sensing of Profiles, NOAA Technical Report ERL 448-WPL 64'. Available from NTIS.

Kaimal, J. C.: 1973, 'Turbulence Spectra, Length Scales and Structure Parameters in the Stable Surface Layer', *Boundary-Layer Meteorol.* **4**, 289–309.

Kondo, J., Kanechika, O., and Yasuda, N.: 1978, 'Heat and Momentum Transfers under Strong Stability in the Atmospheric Surface Layer', *J. Atmos. Sci.* **35**, 1012–1021.

Lumley, J. L., and Panofsky, H. A.: 1964, *The Structure of Atmospheric Turbulence*, Interscience, New York, 239 pp.

Mason, P. J., and Derbyshire, S. H.: 1990, 'Large-Eddy Simulation of the Stably Stratified Atmospheric Boundary Layer', *Boundary-Layer Meteorol.* **53**, 117–162.

McAllister, L. G., Pollard, J. R., Mahoney, A. R., and Shaw, P. J. R.: 1969, 'Acoustic Sounding – A New Approach to the Study of Atmospheric Structure', *Proc. IEEE* **57**, 579–587.

Neff, W. D., and Coulter, R. L.: 1986, 'Acoustic Remote Sensing', in D. H. Lenschow (ed.), *Probing the Atmospheric Boundary Layer*, Amer. Meteorol. Soc., Boston, pp. 201–239.

Nieuwstadt, F. T. M.: 1984, 'The Turbulent Structure of the Stable, Nocturnal Boundary Layer', *J. Atmos. Sci.* **41**, 2202–2216.

Nieuwstadt, F. T. M.: 1985, 'A Model for the Stationary, Stable Boundary Layer', in J. C. R. Hunt (ed.), *Turbulence and Diffusion in Stable Environments*, Clarendon Press, Oxford, pp. 149–179.

Panofsky, H. A. and Dutton, J. A.: 1984, *Atmopheric Turbulence*, Wiley, New York, 397 pp.

Sorbjan, Z.: 1986, 'On Similarity in the Atmospheric Boundary Layer', *Boundary-Layer Meteorol.* **34**, 2430–2432.

Tatarskii, V. I.: 1971, *The Effect of the Turbulent Atmosphere on Wave Propagation*, Kefer Press, Jerusalem, 472 pp. [NTIS TT 68-50464].

Tennekes, H. and Lumley, J. L.: 1972, *A First Course in Turbulence*, MIT Press, Cambridge, 300 pp.

Wyngaard, J. C.: 1973, 'On Surface-Layer Turbulence', in D. A. Haugen (ed.), *Workshop on Micrometeorology*, Amer. Meteorol. Soc., Boston, 392 pp.

Wyngaard, J. C.: 1975, 'Modeling the Planetary Boundary Layer – Extension to the Stable Case', *Boundary-Layer Meteorol.* **9**, 441–460.

Wyngaard, J. C.: 1988, 'Structure of the PBL', in A. Venkatram and J. Wyngaard (eds.), *Lectures on Air Pollution Modeling*, Amer. Meteorol. Soc., Boston, 390 pp.

Wyngaard, J. C.: 1992, 'Atmospheric Turbulence', *Ann. Rev. Fluid Mech.* **24**, 205–233.

Wyngaard, J. C. and Coté, O. R.: 1971, 'The Budgets of Turbulent Kinetic Energy and Temperature Variance in the Atmospheric Surface Layer', *J. Atmos. Sci.* **28**, 190–201.

Wyngaard, J. C., Izumi, Y., and Collins, S. A. Jr.: 1971, 'Behavior of the Refractive Index Structure Parameter Near the Ground', *J. Opt. Soc. Amer.* **61**, 1646–1650.

Wyngaard, J. C., Pennell, W. T., Lenschow, D. H., and LeMone, M. A.: 1978, 'The Temperature-Humidity Covariance Budget in the Convective Boundary Layer', *J. Atmos. Sci.* **35**, 47–58.